Band bending within inhomogeneously doped semiconductors with multilevel impurities. II. Examples

Xizhen Yang
National Laboratory for Superlattices and Microstructures, P.O. Box 912, Beijing, China
and Department of Physics, Beijing Normal University, 100875 Beijing, People's Republic of China

Xiaobai Chen
Basic Physics Teaching and Research Section, Beijing Light Industry Institute, 100037, Beijing, People's Republic of China

Ju Qiu
Basic Department of Shenyang Aeronautical Engineering Institute, 110031, Shenyang, People's Republic of China

Qiang Tian, Zhi Li, and Yiwei Zeng
National Laboratory for Superlattices and Microstructures, P.O. Box 912, Beijing, China
and Department of Physics, Beijing Normal University, 100875 Beijing, People's Republic of China
(Received 18 December 1995)

Using the method for calculating the band bending and concentration profiles of a multilevel impurity center in its different charge states within a semiconductor inhomogeneously doped with the impurity proposed in the preceding paper [X. Yang *et al.*, Phys. Rev. B **53**, 13 414 (1996)] to n-type GaP implanted with Ni and Fe ions, respectively, the results were obtained for the samples implanted and annealed under different conditions. Based on the results, a feasible explanation of the deep-level transient spectroscopy spectra of Ni ion-implanted n-type GaP was obtained and an analysis for the Mössbauer spectra of Fe ion-implanted n-type GaP was carried out. [S0163-1829(96)03320-6]

I. INTRODUCTION

The behavior of $3d$ metal impurities in semiconductors is of concern for both theoretical and applied aspects[2–6] because they may have important influences on optical, electrical, and magnetic properties of materials. Usually, a $3d$ impurity may exist in more than one charge states in semiconductors. The charge states of the impurities in a specific sample affect decisively the properties of the sample. So determining the charge states of the impurities and their profiles within the doping layer in a specific sample is very important. With regard to some physical measurements, for example, deep-level transient spectroscopy (DLTS) and Mössbauer spectroscopy, etc., explanation of experimental results depends strongly on the assignments for the charge states of the impurity in the sample. The band bending within the doping layer is critical in explaining the experimental results, particularly for the measurements using so-called junction capacitance techniques such as DLTS. For example, some unusual peaks observed in the DLTS measurements on Ni ion-implanted n-type GaP samples have been analyzed[7] based on a preliminary estimation of the band bendings in the samples. To improve the analysis, a quantitative calculation of band bending and the profiles of individual charge states of the impurity within the samples has to be invoked. In this paper some major improvements to the method used in Ref. 7 will be made and the reasonable results reported. Another sample is an analysis for the results of Mössbauer spectroscopy measurement on Fe ion-implanted n-type GaP obtained by Qiu.[8] It has been observed that within a layer 0–3000 Å from the surface, the total amount of Fe decreases and the ratio between the concentrations of the charge states Fe(d^6) and Fe(d^5) increases as the annealing time increases. An analysis for the results based on calculating band bending within the samples also will be given in this paper.

The explanations of DLTS spectra of Ni ion-implanted n-type GaP under different conditions will be shown in Sec. II. An analysis of experimental results of Mössbauer spectroscopy measurements on Fe ion-implanted n-type GaP will be described in Sec. III. Then in Sec. IV, some problems about the parameters used in the calculations will be discussed. The concluding remarks will be drawn in the final section.

II. ANALYSIS OF DLTS SPECTRA OF Ni ION-IMPLANTED n-GaP

A. Experimental results and problem

The DLTS spectra of Ni ion-implanted n-type GaP with different implanting conditions have been measured.[7] The substrates used are liquid-encapsulated Czochralski (LEC) n-GaP:S with free-carrier concentrations in the range $n=(3–5)\times10^{17}$ cm^{-3}. The implanting energy was 160 KeV. The dose ϕ, annealing temperature T_A, and annealing time t_A used for the samples are listed in Table I. After implanting and annealing, a Au contract was deposited on the implanted face and an Ohmic contact was made on the rear face to fit the requirement of DLTS measurement. The apparent activation energies E_a and concentrations N_t of the relevant levels observed are also listed in Table I.

It is generally believed that Ni substitutes Ga in GaP and may have three configurations: d^7, d^8, and d^9, corresponding

TABLE I. GaP:Ni sample conditions and comparison between the results of DLTS measurement and calculations. ϕ: dose; T_A: annealing temperature; t_A: annealing time; E_a: apparent activation energy; T_t: concentration; M: majority trap; m: minority trap.

Sample	ϕ (10^{11} cm^{-2})	T_A (°C)	t_A (min)	Levels (Expt.) E_a (eV)	Levels (Expt.) N_t (cm^{-2})	Tentative assign.	$e^t(T)$ behavior	Calculated results $\Delta n(d^j)$ (cm^{-2})	Calculated results Type	Confirmed assign.
11B	1			1.15 (M6)	4×10^{15}	d^9/d^8	$\sim D5$[a]	$\Delta n(d^9)\leqslant5\times10^{15}$	M	d^9/d^8
11T	1	950	30	0.63 (m2)	3×10^{15}	d^8/d^7	Unlike PK[b]	$\Delta n(d^7)<0$		Not Ni_{Ga}
14B	1000			0.62 (M4)	4×10^{16}	d^8/d^7	$\sim PK$	$\Delta n(d^7)\leqslant1.8\times10^{18}$	M	d^8/d^7
14R	1000	700	2	0.61 (M3)	6×10^{16}	d^8/d^7	Unlike PK	$\Delta n(d^7)\leqslant1.8\times10^{18}$	M	Not Ni_{Ga}
14T	1000	950	30	0.60 (ml)	1.2×10^{15}	d^8/d^7	$\sim PK$	$\Delta n(d^7)\leqslant1.5\times10^{16}$	M	Not Ni_{Ga}

[a]$D5$: the electron thermal emission rate data, $e_n^t(T)$, for the GaP:Ni(d^9/d^8) level, cited from Ref. 11.
[b]PK: the hole thermal emission rate data, $e_p^t(T)$, for the GaP:Ni(d^8/d^7) level, cited from Ref. 10.

to two levels $E1=E(d^8/d^7)$ at $E_V+0.62$ eV (Ref. 9) or $E_V+0.51$ eV (Ref. 10) and $E2=E(d^9/d^8)$ at $E_C-0.82$ eV.[11] The latter one has $E_a=1.15$ eV for electron emission, due to its large lattice relaxation behavior. Several levels among those listed in Table I have their E_a near the value of $E1$. They are two majority traps: 0.62 eV ($M4$) in 14B, 0.61 eV ($M3$) in 14R; and two minority traps: 0.63 eV ($m2$) in 11T and 0.60 eV ($m1$) in 14T. Whereas the $M6$ level observed in sample 11B has $E_a=1.15$ eV that is equal to the value of $E2$. These tentative assignments are also listed in Table I. Usually, to confirm an assignment for a level observed experimentally, one makes a comparison between the measured thermal emission rates of the level at different temperatures, $e^t(T)$, and the relevant data have previously been known. Unfortunately, as we shall see later, sometimes this can give a misassignment to the levels. In order to discern if the levels are really caused by Ni_{Ga}, it is necessary to know the band bending, the concentration profiles of the relevant charge states of Ni within the doping layers, and their variations during the DLTS measurement circle (the process of injection bias→reverse bias, V_R). To obtain this information a calculation on the samples has been carried out by using the method described in Ref. 1.

B. Calculation and analysis

For a DLTS measurement,[12] what we need to be especially concerned with is the transition between the different charge states of relevant impurities within the active regions after turning the bias from injection (0 V in our case) to reverse (V_R). Within an active region, if the concentration profile of the jth charge state of the impurity is $n_j^0(x)$ under zero bias, and $n_j^R(x)$ under V_R, then the partial concentration profile of the impurity center in its jth charge state, which can make a contribution to the DLTS spectra, is

$$\Delta n_j(x)=n_j^0(x)-n_j^R(x) \tag{1}$$

and Δn_j is called the active concentration of the charge state. Using the method described in Ref. 1, $n_j^0(x)$ and $n_j^R(x)$ can be calculated, respectively. Then $\Delta n_j(x)$ can be obtained from Eq. (1). Calculated results for samples 11B and 14T are shown in Figs. 1 and 2, respectively. The parameters used in the calculations are $E_g(\mathrm{GaP})=2.26$ eV, the relative dielectric constant $\epsilon_r(\mathrm{GaP})=9$, and the shallow donor (S) level $E_D=E_C-0.104$ eV. These values are accepted commonly for GaP. And $E1=E_V+0.62$ eV,[9] $E2=E_C-0.82$ eV.[11] The

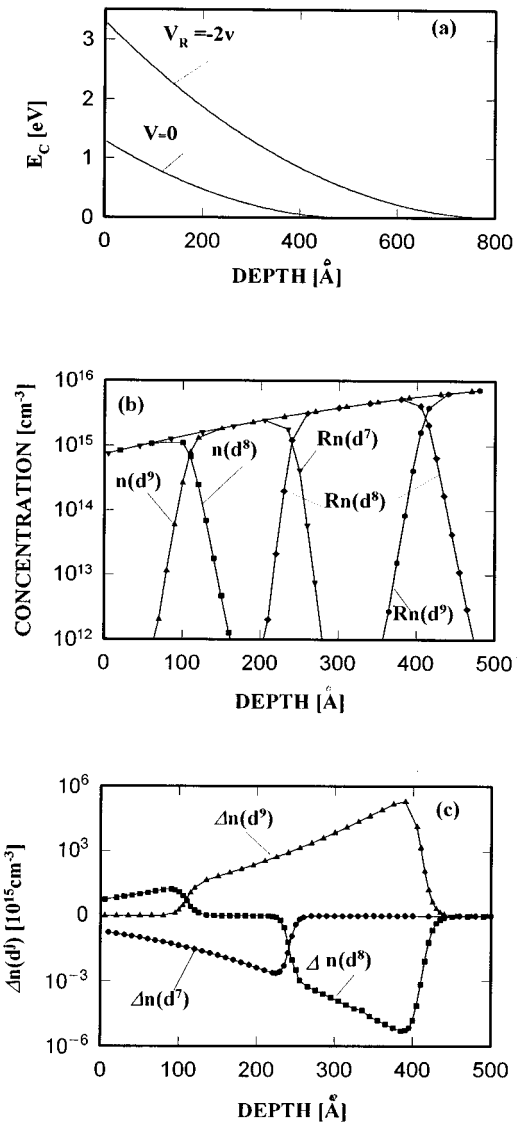

FIG. 1. Results calculated for sample GaP:Ni 11B. (a) Band bending $E_C(x)$; (b) profiles of Ni in its different charge states ($j=7,8,9$). $n(d^j)$: under zero bias [$n(d^7)(x)<10^{11}$ cm^{-3}, so it cannot be seen in the figure]; $Rn(d^j)$: under the reverse bias ($V_R=-2$ V); (c) profiles of active concentrations of the different charge states $\Delta n(d^j)(x)$.

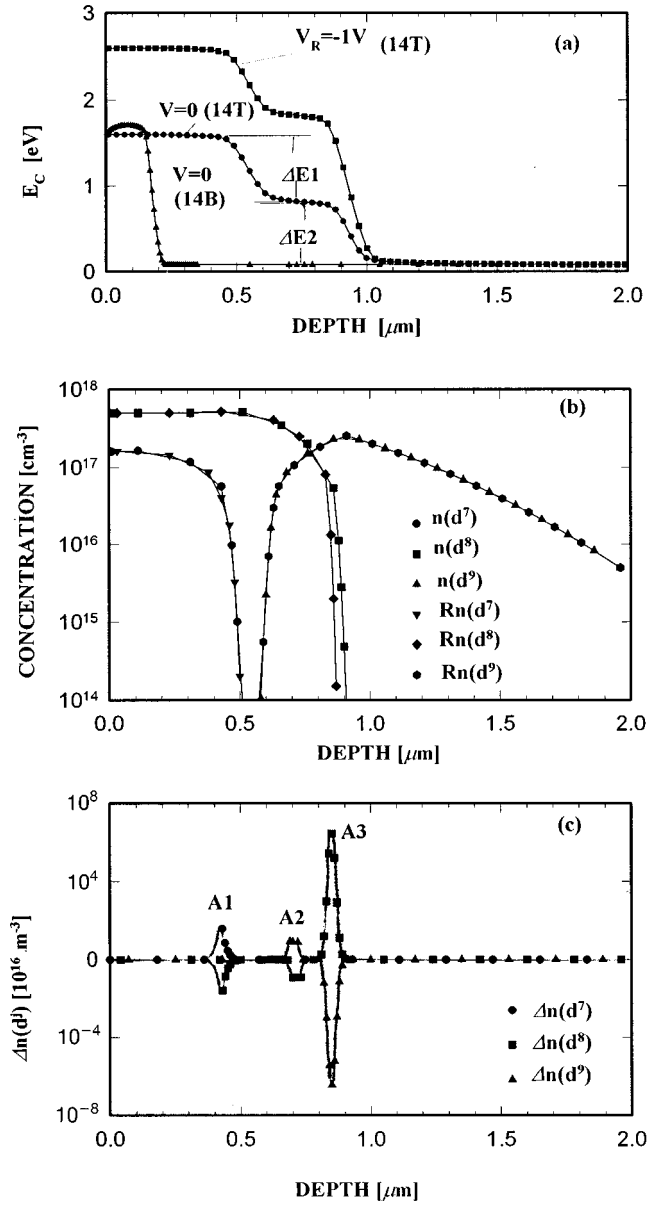

FIG. 2. Results calculated for samples GaP:Ni 14B and 14T. (a) Band bending $E_C(x)$; (b) profiles of Ni in its different charge states (j=7,8,9) for 14T. $n(d^j)$: under zero bias; $Rn(d^j)$: under the reverse bias ($V_R=-4$ V); (c) profiles of active concentrations of the different charge states $\Delta n(d^j)(x)$, for 14T.

profile of implanted ions $N(x)$ before annealing was calculated based on Lindhard-Scherff-Schiott theory.[13] Taking the diffusion effect during annealing into account, it becomes[14]

$$N(x,t)=\frac{\phi}{\sqrt{\pi}\sqrt{2(\Delta R_p)^2+4Dt_A}}\exp\left[-\frac{(x-R_p)^2}{2\Delta R_p^2+4Dt_A}\right], \tag{2}$$

where R_p is the average projected range of the implanted ion in the target and ΔR_p is its standard deviation. For Ni ion implanting into GaP at 160 keV, R_p=812 Å and ΔR_p=343 Å (Ref. 15) were used. D is the diffusion coefficient; its values $D=1\times10^{-12}$ cm^2/sec (950 °C) and 3.8×10^{-15} cm^2/sec (700 °C) were used. A discussion about the values of $E1$ and D will be made in Sec. IV. For calculating a band bending, which is denoted as $E_C(x)$ in this paper, the Fermi level E_F in the sample is taken as the zero point of energy.

1. Samples 11B and 11T

The results for sample 11T have similar features as those for sample 11B shown in Fig. 2. The main difference between them is that the values $n(d^j)$ (j=7,8,9) in 11T are smaller than the corresponding values in 11B by around one order of magnitude. For the sake of brevity, the results for 11T are not shown.

It can be seen from Fig. 1 that samples 11B (and 11T) are still n type. A Schottky barrier is formed near the surface due to contact with Au. This barrier is plotted in Fig. 1(a) based on an ideal Schottky model; the barrier height was taken to be 1.3 eV.[16] Compensation effect of the Ni acceptor has been neglected because the $N(x)$ is lower than the background donor concentration by about two orders of magnitude in the two samples 11B and 11T. The same reverse bias $V_r=-2$ V was used for the two samples. It can be seen from Fig. 1 that within the region of ~0–400 Å from the surface in the two samples, there is a positive space-charge region (PSCR). The active impurity reactions for DLTS measurement in this region are

$$\mathrm{Ni}(d^9)\rightarrow\mathrm{Ni}(d^8)+e_{\mathrm{CB}} \quad \text{(reaction a)}$$

and

$$\mathrm{Ni}(d^8)\rightarrow\mathrm{Ni}(d^7)+e_{\mathrm{CB}} \quad \text{(reaction b)},$$

where e_{CB} stands for an electron in the conduction band. It can be seen from Fig. 1(c) that reaction b happened within the range of 0–100 Å from the surface. The E_a for reaction b is estimated to be about 1.6 eV, which is beyond the measurable range of our experiment. Therefore, it is natural that none of the levels observed in the sample could be connected to the reaction. Reaction a has an activation energy 1.15 eV as described above, which is equal to the value of $M6$ observed in sample 11B. From this point of view, $M6$ may be caused by level Ni (d^9/d^8). On the other hand, in sample 11T, the total amount of the same active impurity center, $\int\Delta n(d^9(x))dx$, is lower than that in 11B by almost one order of magnitude. This may be the reason the same level could not be observed in 11T. The minority level $m2$ (0.63 eV) observed in sample 11T would be caused by the reverse process of reaction b

$$\mathrm{Ni}(d^7)\rightarrow\mathrm{Ni}(d^8)+h_{\mathrm{VB}} \quad \text{(reaction c)}$$

if it was caused by $\mathrm{Ni_{Gu}}$, where h_{VB} stands for the hole in the valence band. Inspecting Fig. 1(c), no such reaction happened in sample 11B (and 11T). Therefore, it can be concluded that $m2$ does not stem from $\mathrm{Ni_{Ga}}$.

2. Samples 14B, 14R, and 14T

As can be seen from Fig. 2, sample 14T is divided into three regions. Within the region $x<4100$ Å, the total nickel concentration $N(x)$ is high enough, up to $\sim8\times10^{17}$ cm^{-3}, to change the region into p type. Within the range $5500<x<9200$ Å, it has become a high resistivity layer (i layer), because of a heavy compensation. When $x>\sim1$ μm, it is still n type due to the very low value of $N(x)$ there. The sample is actually a p-i-n structure [see Fig. 2(a)], which

contains one p-i and one i-n junction. The concentration profiles of Ni in its different charge states under zero bias, $n(d^j)$ ($j=7,8,9$) and those under the reverse bias $Rn(d^j)$ are shown in Fig. 2(b). As can be seen from the figure, $n(d^7)>10^{17}$ cm^{-3} within the region near the Au/GaP interface. The value is much higher than the background shallow donor concentration N_D (5×10^{15} cm^{-3}) and the major portion of $N(x)$ is in d^7 state there. It causes that Fermi level to be almost pinned at the Ni(d^8/d^7) level. This effect is similar to the well-known surface level pinning. Thus, $E_C(x)$ is kept flat within the region. The only exception is a very thin layer close to the Au/GaP interface where the situation might become very complicated, but it has little influence on the problem we are concerned with here so it has been ignored in our calculation. We will discuss this point further in Sec. IV B.

As can be seen from Fig. 2(c), three SCR's, which are active for DLTS measurement, are built up within the sample including two ($A1$ and $A2$) for the p-i junction and one ($A3$) for the i-n junction. Space-charge concentrations in the three SCR's varied during the DLTS measurement circle, and all of them might make their individual contributions to the DLTS spectrum. Corresponding profiles of active impurity concentrations are shown in the figure.

The results for samples 14B and 14R are almost the same and they are similar to those for 14T shown in Fig. 2 but differ from the latter in several aspects: (i) $E_C(x)$ exhibits only one step, unlike the two-step example in sample 14T. In comparison, the calculated $E_C(x)$ for sample 14B is shown in Fig. 2(a) as well. $E_C(x)$ for sample 14R is almost the same as that for 14B so it is not shown in the figure. Consequently, only two SCR's are left as is the situation in the usual p-n junction. The active region $A2$, which is created by the i layer in sample 14T, disappeared in samples 14B and 14R. (ii) The height of the $\Delta n(d^7)(x)$ peak (within active region $A1$) increased by almost two orders of magnitude and the height of the $\Delta n(d^8)(x)$ peak (within active region $A3$) increased by almost one order of magnitude because $N(x)$ in the two samples are concentrated in a much narrower region from the surface due to weaker (for 14R) or no (for 14B) annealing effect. (iii) The depth of the barrier is only around 2000 Å, which is shallower than that in 14T (~1 μm). For the sake of brevity, the relevant results for 14T and 14R are not shown in Figs. 2(b) and 2(c).

It can be seen from Fig. 2(b) that the transition, which takes place in region $A1$, is reaction c. Noting that the region is a negative SCR (NSCR) within the p-i junction, the transition then should cause a majority peak on the DLTS spectrum and its E_a should be equal to 0.62 eV. Indeed, the levels $M4$ and $M3$ were observed in 14B and 14R, respectively. However, there are no such majority peaks on the spectrum of sample 14T. Comparing samples 14B (and 14R) and 14T, the same transition occurs in all three but the active concentration in 14T is lower than that in 14B and 14R by almost two orders of magnitude. This might be the reason that the peak can be observed in 14B ($M4$) and 14R ($M3$) but not in 14T. With respect to 0.60 eV minority level ($m1$) observed in 14T, if it were of Ni_{Ga} origin it would correspond to reaction c and occur in a PSCR. No such reaction can be found in Fig. 2(c). Therefore, the $m1$ level could not be connected to Ni_{Ga}.

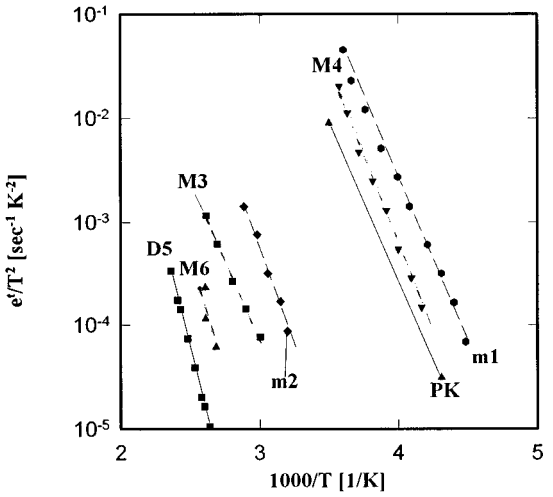

FIG. 3. Arrhenius plot for a comparison between the $e^t(T)$ data measured for the relevant levels and those reported in Ref. 10 (the solid line PK) and in Ref. 11 (the solid line $D5$).

Now we turn to consider the influences of active Ni_{Ga} centers in the other SCR's. They do not manifest themselves on the DLTS spectra for different reasons. For instance, the transition that occurred in region $A3$,

$$\mathrm{Ni}(d^8)\rightarrow\mathrm{Ni}(d^9)+h_{\mathrm{VB}} \quad \text{(reaction d)}$$

has a thermal activation energy larger than ~1.6 eV. It is already beyond the DLTS measurement range. The transition a that occurred in $A2$ has $E_a=1.15$ eV. No corresponding level has been observed in the DLTS spectrum of 14T. One of the possible reasons for this is that some defect reactions occurred during the lengthy thermal annealing, which suppressed the amount of Ni_{Ga} center, so that even though $N(x)$ is still kept the same as that calculated using Eq. (2), both $n(d^j)(x)$ and $\Delta n(d^j)(x)$ have been changed somehow.

3. Temperature dependences of carrier emission rates

Comparing the calculated $\Delta n_j(x)$ and the types of the individual levels observed experimentally in the spectra, the two levels, $m2$ in 11T and $m1$ in 14T have been ruled out from the candidates of Ni_{Ca}. So, among the levels observed in the samples listed in Table I only majority traps $M4$ in 14B, $M3$ in 14R, and $M6$ in 11B might be caused by the Ni_{Ga} center. To clarify this point, the temperature dependences of carrier emission rates, $e^t(T)$, of the relevant levels have been compared to those of Ni(d^8/d^7) and Ni(d^9/d^8) levels published in Refs. 10 and 11, respectively. The data are shown in Fig. 3. It can be seen from the Arrhenius plot that the behavior of the $M4$ level is similar to that of Ni(d^8/d^7) (the solid line PK in the figure), but $M3$ behaves quite differently. Therefore, it can be concluded that the latter is not caused by Ni_{Ga}. It can also be seen from Fig. 3 that the behavior of the $M6$ level observed in the sample 11B is close to that of Ni(d^9/d^8) (the solid line $D5$ in Fig. 3). This supports the correlation between them. Therefore, one can draw a conclusion that only the 0.62 eV ($M4$) level in 14B and 1.15 eV ($M6$) in 11B may be caused by the Ni_{Ga} center, among all of the levels observed experimentally.

TABLE II. Comparison between the results of Mössbauer measurement on GaP:Fe and those calculated.

Sample	Anneal. Time t_A (min)	Experimental results		Calculated results	
		$I(d^6)/I(d^5)$	Total effect	$n(d^6)/n(d^5)$	N_T (cm^{-3})
7-4	4	1.105	1.42	3.62×10^{-3}	1.38×10^{20}
7-60	60	1.352	1.17	1.42×10^{-2}	3.52×10^{19}

III. ANALYSIS OF MÖSSBAUER SPECTRA OF Fe ION-IMPLANTED *n*-TYPE GaP

It is generally believed that Fe may substitute Ga in GaP, and it may exist in three different charge states: Fe(d^5), Fe(d^6), and Fe(d^7). Correspondingly, two levels $E1(d^6/d^5)=E_V+0.86$ eV (Ref. 17) and $E2(d^7/d^6)=E_C-0.26$ eV (Ref. 18) are formed within E_g.

Qiu[8] measured Mössbauer spectra of the Fe ion-implanted LEC GaP:S samples. The free carrier concentration of substrates is $n=5\times10^{17}$ cm^{-3}. Fe ion implanting dose $\phi=7.6\times10^{16}$ cm^{-2}, energy $E=160$ keV, and annealing temperature $T_A=950$ °C. The annealing times t_A for the samples used are collected in Table II.

The results of conversion electron Mössbauer spectroscopy measurements showed that the total effect, which is proportional to the total amount of Fe within the range ~3000 Å from the surface in a sample, decreases as t_A increases. Also the ratio between the concentration of Fe(d^6) and that of Fe(d^5), $I(d^5)/I(d^5)$, increases as t_A increases. The relevant data are also listed in Table II.

Using the method described in Ref. 1, band bending $E_C(x)$ and profiles $n(d^5)(x)$ and $N(d^6)(x)$ were calculated for the samples. The profile of the total implanted Fe ion, $N(x)$, was also calculated by using Eq. (2). The parameters used in the calculations are $R_p=906$ Å, $\Delta R_p=380$ Å,[15] and $D(950\ °C)=1\times10^{-10}$ cm^2/sec.[19] The relevant calculated results are shown in Fig. 4. The profile $N(x)$ is shown in Fig. 4(a). It can be seen from the figure that a reverse layer occurs within both samples, because $N(x)$ has a maximum larger than 10^{19} cm^{-3}, which is much larger than the free-carrier concentration n in both samples. Figure 4(b) shows their $E_C(x)$. Comparing sample 7-4, the longer t_A of sample 7-60

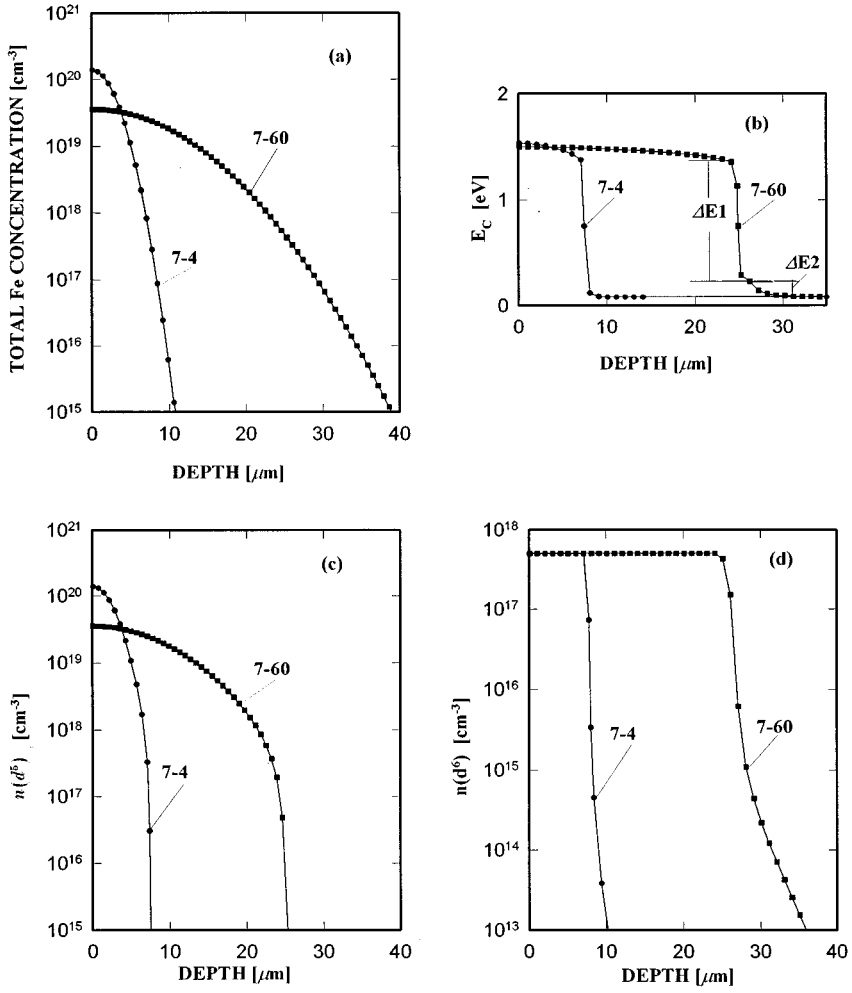

FIG. 4. Results calculated for Fe ion-implanted GaP samples 7-4 and 7-60. (a) Profiles of Fe ion-implanted into the samples; (b) band bending $E_C(x)$; (c) profiles of $n(d^5)(x)$; (d) profiles of $n(d^6)(x)$.

distributed the implanted Fe ions over a wider range. The p-type layer extends to ~ 25 μm from the surface in sample 7-60 and two steps appear on the $E_C(x)$. Because the abscissa scale is very large compared to the step width, the second step is not obvious in the figure, but it can still be recognized. Sample 7-4 has a similar $E_C(x)$ behavior, but the steps on $E_C(x)$ occur at different depths, ~ 7 and ~ 8 μm, respectively.

The calculated $N(x)$ for the two samples are shown in Fig. 4(a). The figure shows that near the surface, the value of $N(x)$ in sample 7-4 is higher than that in sample 7-60. This is in qualitative agreement with that observed in the experiment (see the total effects data listed in Table II). The profiles $n(d^5)(x)$ and $n(d^6)(x)$ are shown in Figs. 4(c) and 4(d), respectively. It can be seen from the two figures that, within a layer near the surface, the value of $n(d^5)(x)$ decreases as t_A increases, but the value of $n(d^6)(x)$ keeps at the same level independent of t_A. Thus, the ratio $n(d^6)(x)/n(d^5)(x)$ within the layer increases as t_A increases. This is in qualitative agreement with the result observed experimentally as well [see the ratios $I(d^6)/T(d^5)$ listed in Table II]. For comparison, the relevant values calculated are listed in the two rows on the right in Table II. Inspecting the data, however, some discrepancies exist in a quantitative view. The ratio of the total amounts of Fe in the two samples measured experimentally (total effect) is only $1.42/1.17 \simeq 1.21$, but the value calculated is $1.38\times10^{20}/3.52\times10^{19} \simeq 3.52$. This difference can be attributed to some experimental factors, for example, the detection sensitivities for the two samples were not the same. On the other hand, the ratios $I(d^6)/I(d^5)$ of the two samples are 1.105 and 1.352, but the calculated ratios $n(d^6)/n(d^5)$ are 3.62×10^{-3} and 1.02×10^{-2}, respectively. Each ratio $I(d^6)/I(d^5)$ was measured on the same sample during the same measurement circle. No problem of sensitivity was involved. By inspecting Fig. 4(d), it can be understood that the values of $n(d^6)$ calculated are limited by the shallow donor concentration $N_D=5\times10^{17}$ cm^{-3}. It is reasonable, because the amount of e_{CB} that can be used to fill the $\mathrm{Fe_{Ga}}(d^6/d^5)$ level, resulting in the transition $\mathrm{Fe}(d^5)\rightarrow n(d^6)$, is just the value of N_D. On the other hand, the values of $n(d^5)$ in the two samples go up to 1.38×10^{20} and 3.52×10^{19} cm^{-3}, respectively. Thus, the calculated ratios $n(d^6)/n(d^5)$ have been suppressed down to the range of 10^{-3}–10^{-2}, which are much smaller than the values measured experimentally. One of the possible reasons for this discrepancy is that a part of the implanted Fe ions has not taken the substitutional site, but stayed at some interstitial sites, due to the use of too large dosage. Considering that the typical solubility limits of $3d$ impurities in III-V compounds are in the range of 10^{17}–10^{18} cm^{-3} (see Ref. 2), this hypothesis is reasonable. Some experimental evidence for the existence of interstitial Fe in GaP has been reported.[20] The interstitial Fe impurity in GaP may act as donors releasing some electrons into the CB. It supplies some extra e_{CB} to be captured by the substitutional $\mathrm{Fe}(d^5)$, resulting in a decrease of $n(d^5)$ and an increase of $n(d^6)$. This causes the ratio $n(d^6)/n(d^5)$ to be increased. In other words, comparing the results measured experimentally and those calculated, the discrepancy indicates that only a part, but not all, of the implanted Fe ions has taken the substitutional sites. A detailed analysis for the problem is out of the scope of the present paper. More work is needed to get a consistent analysis. Another possible factor responsible for the discrepancy is the surface barrier. This point will be discussed in Sec. IV B.

IV. DISCUSSION

A. Shape of $E_C(x)$

In Ref. 1, the band bendings within a semiconductor layer doped inhomogeneously with a multilevel impurity have been classified into three types: multisteplike, single-steplike, and the others (no obvious bending), depending on the profile of the impurity. For sample 14B of GaP:Ni, the total concentration of Ni is high enough and annealing is sufficient, then two steps appear on the $E_C(x)$, and the whole sample is actually a p-i-n structure [see Fig. 2(a)]. Combining Figs. 2(a), 2(b) and 2(c), it can be seen that the p-i step is caused by the transition from $\mathrm{Ni}(d^7)$ to $\mathrm{Ni}(d^8)$, and the i-n step is a result of that from $\mathrm{Ni}(d^8)$ to $\mathrm{Ni}(d^9)$, as described in Ref. 1. The transition from $n(d^8)(x)$ to $n(d^9)(x)$ is quite slow [see the region $x \simeq 7500$–8500 Å in Fig. 2(b)]. The height of the first step (at around $x\sim5000$ Å), $\Delta E1$, is equal to the difference between levels $\mathrm{Ni}(d^9/d^8)$ and $\mathrm{Ni}(d^8/d^7)$, $E2-E1=0.81$ eV. The height of the second step (at around $x\sim1$ μm), $\Delta E2$, is equal to the difference between E_F in the neutral n layer and level $E(d^9/d^8)$. That is $\Delta E2 \simeq E_D-E2=0.716$ eV. In the calculation described above, the value of $E1$ was taken to be Fung's data, $E1=E_V+0.62$ eV.[9] If the value reported by Peaker *et al.*,[10] $E1=E_V+0.51$ eV, is used, then the following changes in the calculated $E_C(x)$, $n(d^j)(x)$, and $\Delta n(d^j)(x)$ will be introduced: (i) The height of the first step on $E_C(x)$, $\Delta E1$, will be changed from 0.81 to 0.92 eV, still being equal to the difference $E2-E1$. (ii) While profiles $E_C(x)$, $n(d^j)(x)$, and $\Delta n(d^j)(x)$ keep their main features such as the number of the steps on $E_C(x)$, the numbers and sequence of PSCR's, NSCR's, and the active impurity reactions, etc., the characteristic depths at which the steps occur and the values of $n(d^j)(x)$ and $\Delta n(d^j)(x)$ will be changed somewhat. However, these changes do not contradict the explanation described in Sec. II B.

Qiu's GaP:Fe samples 7-4 and 7-60 belong to this type, as well. For GaP:Fe, $E1=E_V+0.86$ eV and $E2=E_C-0.26$ eV, so $\Delta E1 \simeq 1.14$ eV and $\Delta E2 \simeq 0.16$ eV [see Fig. 4(b)].

Every transition between two adjacent charge states results in a DLTS active reaction, so an active region is formed. For example, in sample 14T, the first step on $E_C(x)$ corresponds to the transition $\mathrm{Ni}(d^7)\rightarrow\mathrm{Ni}(d^8)$ [see Fig. 2(b), ~0.5 μm). When the reverse bias is applied during the DLTS measurement, the step extends into the p-type region. This causes $E_C(x)$ within the extended region to be lowered somewhat related to E_F (or to the quasi-Fermi level under reverse bias). The $\mathrm{Ni_{Ga}}$ levels were lowered correspondingly, making an increase in the occupancies of the levels. The most violent change should occur on level $\mathrm{Ni}(d^8/d^7)$, because E_F was pinned there before reversing the bias. In other words, the transition $\mathrm{Ni}(d^7)\rightarrow\mathrm{Ni}(d^8)$ is the prominent one there. The region is just $A1$ in Fig. 2(c). A similar event takes place within region $A3$, where the SCR extends into the i layer somewhat when the reverse bias is applied. Considering E_F was pinned at the level $\mathrm{Ni}(d^9/d^8)$ and $E_C(x)$ was lowered there, the transition should be $\mathrm{Ni}(d^8)\rightarrow\mathrm{Ni}(d^9)$.

That is just what occurred within $A3$ in Fig. 2(c). In regard to $A2$ in the figure, this corresponds to an extension of the first step on $E_C(x)$ into the i layer when the reverse bias is turned on. This raises $E_C(x)$ and the occupancy of level Ni(d^9/d^8) decreases. So the transition that occurred in the region should be $(d^9)\rightarrow(d^8)$, as shown in Fig. 2(c). It is worthy to note that only three active regions appear in the sample. The other active region that would occur in the n side of the i-n junction is lost. Along the same lines of analysis, it can be found that $E_C(x)$ rises there when the reverse bias is turned on. What would happen is a decrease of the occupancy of the Ni_{Ga} center. In fact, the occupancy cannot decrease obviously, because E_F was located far above the level Ni(d^9/d^8) there, so almost all of the Ni_{Ga} are still in the configuration Ni(d^9). Therefore the fourth active region for the Ni_{Ga} center cannot occur. Of course, a PSCR still exists within the region, but it is caused by the variation of the occupancy of the shallow donor center.

When the dopant's concentration in a sample is high enough and its profile is steep enough, the $E_C(x)$ will be single-step-like, as pointed out in Ref. 1. GaP:Ni sample 14B belongs to this type, as can be seen from Fig. 2(a). When x is larger than 1600 Å, $E_C(x)$ falls down quickly. Within the junction region, charge-state transitions $d^7\rightarrow d^8\rightarrow d^9$ are completed in sequence. So $n(d^9)$, but not $n(d^8)$ as in the case of sample 14T, increases very rapidly and becomes the dominant charge state of Ni.

A discussion on the active region similar to that for sample 14T can be made for sample 14B, as well. The only difference is that the second step on $E_C(x)$ is hidden as described above. It results in the disappearance of the active region corresponding to $A2$ in 14B; then only two active regions can be found in the sample. They are similar to $A1$ and $A3$ in 14T shown in Fig. 2(c), but occur at ~1400 and ~1700 Å from the surface, respectively.

As discussed in Ref. 1, when the doping level is very low, the impurity mainly acts as a compensator, but does not cause any obvious band bending. Roughly speaking, the situation in samples 11B and 11T of GaP:Ni described in Sec. II B 1 belong to this type [see Fig. 1(a)] because $N(x)\leqslant 10^{15}$ cm^{-3} in 11T and $N(x)\leqslant 5\times10^{15}$ cm^{-3} $(=N_D)$ within the majority of the implanted layer in 11B.

B. Influence of the Schottky barrier near the surface

A Schottky barrier near the surface always exists in all of the GaP:Ni samples described in Sec. II, due to the Au contact deposed on the surface. For samples 11B and 11T, as mentioned in the preceding paragraph, the Schottky barrier has the dominant role, and it has been taken into account in the calculation described in Sec. II B 1. But it has been ignored in the calculations for the other samples described in Sec. II B 2. The problem with the Schottky barrier near the surface in samples 14B, 14R, and 14T should be discussed here. The layer near the surface has been changed to p type in the samples. The barrier will be an Au p-type GaP Schottky barrier, if it appears. It will result in decreasing $E_C(x)$ somewhat within the barrier region when the sample is under zero bias. While the nominal reverse bias is applied on the sample during the DLTS measurement, the Schottky barrier is actually under a forward bias, because the Au electrode is connected to the negative electrode of the source, and the rear face of the substrate is connected to the positive electrode in the experiment. Thus, the barrier will be lowered. In other words, $E_C(x)$ will rise related to E_F within the barrier region. The corresponding charge-state transition of the Ni_{Ga} center within the region should be $(d^9)\rightarrow(d^8)$ and/or $(d^8)\rightarrow(d^7)$. Both of the two transitions have their $E_a\geqslant 1.1$ eV. The values are too large compared to the value $E_a\simeq 0.60$–0.70 eV, which is of concern within the analysis for the samples (see Table I). Therefore, it does not cause any changes to the conclusions made on the samples in Sec. II B 2 and Sec. II B 3. So ignoring the Schottky barrier in the analyses for the three samples is reasonable.

With regard to the GaP:Fe samples discussed in Sec. III, no Schottky barrier exists near the surface because there is no Au contract. But a surface barrier may exist. The barrier might affect the conduction-band electron concentration n within the layer near the surface. For example, if the barrier should be a hole barrier, then n will be raised within the barrier region. This will increase $n(d^6)$ and decrease $n(d^5)$. Thus, the discrepancy between the results calculated and those measured experimentally will be remedied in a sense. A detailed analysis for this effect is difficult because of the shortage of relevant information.

C. Diffusion coefficient

With regard to the values of the diffusion coefficients, for the GaP:Ni samples $D(950\,^\circ\text{C})=1\times10^{-12}$ cm^2/sec and $D(700\,^\circ\text{C})=3.8\times10^{-15}$ cm^2/sec were used, respectively, in the calculation described in Sec. II. Adjusting the values, the results obtained indicate that, within the ranges 2.8×10^{-13}–1.7×10^{-12} cm^2/sec for $D(950\,^\circ\text{C})$ and $(0$–$8.3)\times10^{-14}$ cm^2/sec for $D(700\,^\circ\text{C})$, the features $E_C(x)$ and $n(d^j)(x)$, such as the number of steps on $E_C(x)$ and their heights, the number of SCR and their polarities and the types of DLTS active concentrations in the individual SCR's have not been changed. What has been changed are the positions (depth from the surface) of the steps on $E_C(x)$ and amounts of the space charges within the individual SCR's. These changes are limited in a certain degree so that the conclusions on the GaP:Ni samples given above are still held.

In general, a diffusion coefficient is thermally active:

$$D(T)=D_0\exp(-Q/kT). \tag{3}$$

By fitting the relation with the values of D used in the calculations, the values $Q=2.286$ eV and $D_0=2.6\times10^{-3}$ cm^2/sec are obtained.

For the GaP:Fe samples, the values of the diffusion coefficients used are $D(950\,^\circ\text{C})=1\times10^{-10}$ cm^2/sec and $D(900\,^\circ\text{C})=4\times10^{-11}$ cm^2/sec. These values can also be adjusted within a certain range, keeping the qualitative behaviors of the calculated $E_C(x)$ and $n(d^j)(x)$ as the same obtained in the calculations described in Sec. III.

Baranowski, Jezewski, and Liro[19] reported that $D(1200\,^\circ\text{C})=1.5\times10^{-6}$ cm^2/sec for GaP:Ni. Shishiyanu and Giorgiu[21] reported a relation for GaP:Fe between 980 and 1180 °C,

$$D_{\text{eff}}=0.66\,\exp\left(-\frac{2.3\pm0.2\ \text{eV}}{kT}\right).$$

Comparing these data, some inconsistency seems to exist. Further work needs to be done to get consistency.

D. Significance of the calculation

Usually, one makes assignments to the levels measured by DLTS in two ways. The preliminary way is to consider simply the apparent activation energy E_a as the critical value. The second way is based on a comparison between the data $e^t(T)$, which have been called the ''fingerprint'' of a level, and those that have already been known. Of course, this method is much more reliable than the preliminary one. But it is still not unambiguous. For example, the electric field effect on the emission rates (Poole-Frenkel effect) may cause E_a lowering $\sim$20%,[22,23] and the strengths of the electric field within the active regions in the samples used in different experiments are not easy to keep identical. Additionally, the situation will become more complicated for the multilevel impurities, because the influences of the effect are quite different for the different charge states.[24] By using the scheme we proposed in this paper, the concentration profiles of the impurities in their individual charge states can be calculated. This gives another criterion to distinguish whether or not a level observed experimentally is connected with a specific impurity. For example, in the Ni ion-implanted n-type GaP samples, as can be seen from Table I, all of the levels $m1$, $m2$, $M3$, and $M4$ could be tentatively assigned to be $\mathrm{Ni}_{\mathrm{Ga}}(d^8/d^7)$ according to their values E_a. By comparing behaviors of $e^t(T)$, both $m2$ and $M3$ can be ruled out from the candidates, but the $e^t(T)$ data of level $m1$ in 14T are not too far away from those of $\mathrm{Ni}_{\mathrm{Ga}}(d^8/d^7)$ reported in Ref. 10 (line PK in Fig. 3). Thus, whether or not $m1$ has originated from $\mathrm{Ni}_{\mathrm{Ga}}$ remains questionable. The calculation for sample 14T indicates that the active concentration $\Delta n(d^7) \leqslant 1.5\times10^{16}$ cm^{-3}, which is acceptable for assigning the level to $\mathrm{Ni}(d^8)/d^7)$ providing the corresponding level is a majority trap. $m1$ is a minority trap, however, thus the conclusion that $m1$ is not connected with $\mathrm{Ni}_{\mathrm{Ga}}$ can be drawn. This is an example exhibiting the significance of the calculation scheme proposed in this work.

Another example shown in Sec. 3, the analysis of the Mössbauer measurement results of Fe ion-implanted n-type GaP, indicates that a comparison between the results measured experimentally and those calculated explores an obvious discrepancy in a quantitative sense. This gives a hint as to the question of which crystalline sites were taken up by the implanted Fe ions.

V. CONCLUSIONS

The calculation scheme proposed in Ref. 1 has been used to calculate $E_C(x)$ and $n(d^j)(x)$ for n-type GaP implanted with Ni ions under different conditions. The results can be used to explain the feasibility of the DLTS spectra and judge the assignments of the levels.

The same scheme has been used to calculate $E_C(x)$ and $n(d^j)(x)$ for the n-type GaP samples implanted with Fe ions used in the Mössbauer measurement. A comparison between the results measured and those calculated gives some indication that a part of the implanted Fe ions has taken up interstitial sites.

These examples have confirmed the classification of the band bending in a semiconductor layer doped inhomogeneously with a multilevel impurity described in Ref. 1 and shown that the scheme is significant in a quantitative analysis of the experimental results.

[1] Xizhen Yang, Zhi Li, and Qiang Tian, preceding paper, Phys. Rev. B **53**, 13 414 (1996).

[2] A. M. Hennel, in *Semiconductors and Semimetals* Vol. 38, edited by R. K. Williams, A. C. Boer, and E. R. Weber (Academic, New York, 1993), Chap. 5.

[3] A. Zunger, in *Solid State Physics* Vol. 39, edited by H. Ehrenreich and D. Turnbull (Academic, New York, 1986).

[4] E. M. Omel'yanovskii and V. I. Fistul', *Transition Metal Impurities in Semiconductors*, translated from Russian by A. Tybulewicz (Adam Hilger, Bristol, 1985).

[5] A. E. Carlson, in *Solid State Physics* Vol. 43, edited by H. Ehrenreich and D. Turnbull (Academic, New York, 1990).

[6] J. Dreyhsig, H.-E. Gumlich, and J. W. Allen, Phys. Rev. B **48**, 15 002 (1993).

[7] Xizhen Yang and Xiaobai Chen (unpublished).

[8] Qiu Ju, Diploma, Beijing Normal University, 1988 (unpublished).

[9] S. Fung and R. J. Nicholas, J. Phys. C **15**, 7355 (1982).

[10] A. R. Peaker, U. Kaufmann, Zhan-Guo Wang, R. Wöorner, B. Hamilton, and H. G. Grimmeiss, J. Phys. C **17**, 6161 (1984).

[11] Xizhen Yang and J. W. Allen, Semicond. Sci. Technol. **6**, 243 (1991).

[12] D. V. Lang, J. Appl. Phys. **45**, 3023 (1974).

[13] J. M. Lindhard, M. Scherff, and H. E. Schiott, Mat. Fys. Medd. K. Dan. Vidensk. Selsk, Matt-Fys. Medd. **33**, (14) (1963).

[14] LI Guohui, Wang Xingmin, Lu Zhiheng, Zhang Tonghe, and Tian Shuyun, Chin. J. Semicond. **4**, 374 (1983).

[15] J. F. Gibons, W. S. Johnson, and S. W. Mylroie, *Projected Range Statistics*, 2nd ed. (Dowden, Hutchingson & Ross, Stroudsburg, PA, 1975).

[16] I. Imeishi, I. Hamakawa, and N. Shilahuji, Phys. Prop. Semicond. Zhaotzan **II**, 44 (1977) (in Japanese).

[17] X. Z. Yang, H. G. Grimmeiss, and L. Samuelson, Solid State Commun. **48**, 427 (1983).

[18] K. Suto and J. Nishizawa, J. Appl. Phys. **43**, 2247 (1972).

[19] J. M. Baranowski, M. Jezewski, and Z. Liro, Physica **117B/118B**, 179 (1983).

[20] P. P. Seregin, F. S. Nasredinov, and A. Sh. Bathtiyasov, Phys. Status Solidi B **91**, 35 (1979).

[21] F. S. Shishiyanu and V. G. Georgiu, Fiz. Tekh. Polaprovodn. **10**, 2188 (1976) [Sov. Phys. Semicond. **10**, 1301 (1976)].

[22] S. D. Brotherton and A. Gill, Appl. Phys. Lett. **33**, 953 (1978).

[23] N. Baber, H. Scheffler, A. Ostmann, T. Wolf, and D. Bimberg, Phys. Rev. B **45**, 4043 (1991).

[24] Ma Hong, Yang Xizhen, Zhou Jie, Lu Liwu, and Feng Songlin, Chin. J. Semicond. **16**, 574 (1995).